The transition state in the isomerization of rhodopsin

La Penna, G.; Buda, F.; Bifone, A.; Groot, H.J.M. de

25 September 1998

ELSEVIER

Chemical Physics Letters 294 (1998) 447–453

CHEMICAL PHYSICS LETTERS

The transition state in the isomerization of rhodopsin

Giovanni La Penna [a,1], Francesco Buda [a,*], Angelo Bifone [b], Huub J.M. de Groot [c]

[a] *Istituto Nazionale per la Fisica della Materia, Laboratorio Forum, Scuola Normale Superiore, Piazza dei Cavalieri 7, I-56126 Pisa, Italy*
[b] *Magnetic Resonance Research Group, The Institute of Cancer Research, The Royal Marsden NHS Trust, Downs Road, Sutton, Surrey SM2 5PT, UK*
[c] *Leiden Institute of Chemistry, Gorlaeus Laboratoria, University of Leiden, 2300 RA Leiden, The Netherlands*

Received 10 January 1998; in final form 20 July 1998

Abstract

We present an ab-initio molecular dynamics study of a model of the chromophore of rhodopsin. The 11-*cis* to all-*trans* ground-state isomerization of a retinylidene–ethylimine · HCl has been induced by applying an external classical force field to the C10–C11–C12–C13 dihedral angle, in addition to the ab-initio forces. By using this hybrid approach, we find that the transition state is characterized by a well-defined bond pattern along the chromophore and by a positive charge displacement. The relaxation of the chromophore is associated with propagation of a conjugation defect that transports the excess positive charge along the backbone.

1. Introduction

The primary event in vision is the photoconversion of a 7-helix membrane protein, rhodopsin, to a metastable intermediate, bathorhodopsin [1,2]. The chromophore of rhodopsin is an 11-*cis* retinylidene prosthetic group linked to the side chain of Lys^{296} of the opsin protein via a protonated Schiff base (see Scheme 1). The absorption of a photon by the chromophore induces the isomerization of the C11–C12 bond from a *cis* to *trans* conformation (bathorhodopsin). The photoconversion is completed in about 200 fs [3] and is characterized by a quantum yield of 65% [4]. At physiological conditions, the primary photoproduct, bathorhodopsin, quickly decays through several intermediates. These processes initiate a chain of biochemical reactions that lead to the closing of the sodium channels in the cell membrane. The energy conversion in the primary event is remarkably efficient, as $\simeq 60\%$ of the energy of the absorbed photon (32 kcal/mol) is stored in the primary photoproduct [5,6].

A great deal of work has been devoted to the study of the dynamics of rhodopsin in the lowest-lying Frank–Condon excited state, which is involved in the photoisomerization process [1,7]. A much less investigated aspect is the dynamics of the isomerization in the ground state. Besides its relevance to the thermal isomerization of rhodopsin [8,9], the ground-state energy saddle point is interesting for the study of the relaxation of the chromophore towards the primary photoproduct. According to the current picture of the photoisomerization process, the

* Corresponding author. E-mail: buda@aix6.cmp.sus.it
[1] Current address: CNR, Istituto di Studi Chimico-Fisici di Macromolecole Sintetiche e Naturali, Via de Marini 6, I-16149 Genova, Italy.

0009-2614/98/$ - see front matter
PII: S0009-2614(98)00870-7

chromophore oscillates in a local minimum in the excited-state potential surface. When the C10–C11–C12–C13 dihedral angle goes through the orthogonal region, the system is transferred to the ground state in a barrierless non-radiative transition [3,7] and relaxes either to the primary photoproduct (all-*trans* bathorhodopsin) or to the initial configuration (11-*cis*). The relaxation of the chromophore toward the photoproduct is determined by the ground-state potential energy surface in the vicinity of the transition state.

In this Letter, we present a Car–Parrinello molecular dynamics (CP-MD) [10,11] study of the isomerization on the ground-state potential. We impose an external torsional field to the C10–C11–C12–C13 dihedral angle to force the system along the reaction coordinate. In Fig. 1 we show the full cycle of configurations explored during the direct and inverse isomerization of the chromophore. When the system approaches the transition state, we observe a crossing of the Kohn–Sham electron energy levels that results in a characteristic sharp increase in the fictitious electronic kinetic energy [12]. We find that the transition states for the *cis*-to-*trans* and the *trans*-to-*cis* isomerizations are characterized by a displacement of the positive charge and the associated conjugation defect, rather than by a specific C10–C11–C12–C13 dihedral angle. This displacement results in a characteristic bond pattern and inversion of the bond alternation in the tail of the molecule. Relaxation from the transition state to the all-*trans* or to the 11-*cis* photoproducts is associated with a coherent propagation of the conjugated defect which transports the positive charge along the backbone. Recent CP-MD studies have shown that the conjugated backbone of the chromophore supports soliton-like excitations [13]. The present results show that the coherent propagation of the charged defect is intrinsic to the

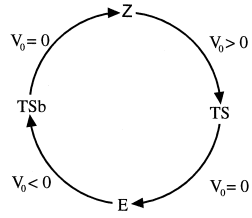

Fig. 1. Cycle of configurations during the direct and subsequent inverse isomerization of the chromophore. Z denotes the starting 11-*cis* configuration (rhodopsin). The external force field V_0 drives the system to the transition state TS. After the transition state has been reached, the applied potential is set to zero, and the system evolves under the effect of internal forces only towards the all-*trans* configuration E (bathorhodopsin). An external potential $-V_0$ is then applied to force the back-isomerization. The new transition state is denoted by TSb.

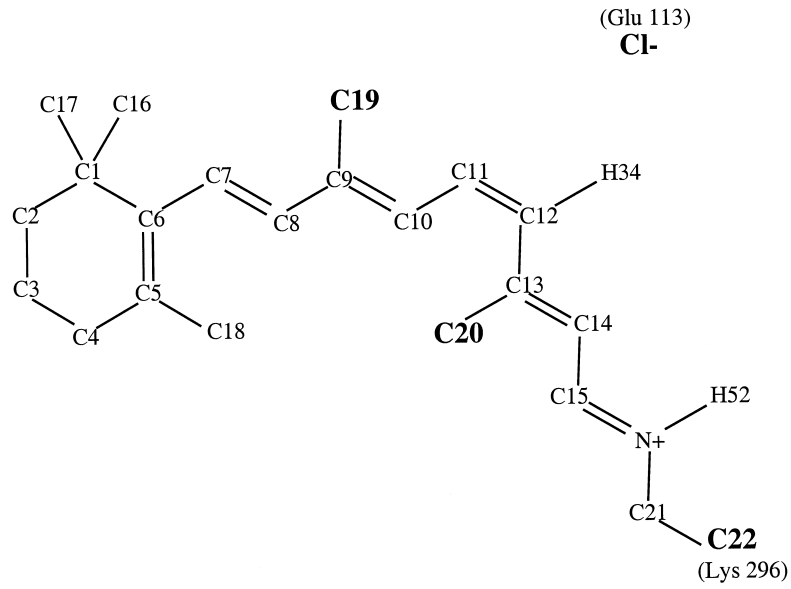

Scheme 1.

relaxation of the chromophore toward the photoproduct. The propagation of this charged soliton should be detectable in transient absorption spectroscopy.

2. Computational method and technical details

In ab-initio molecular dynamics [10,11] the interatomic forces are computed from the instantaneous quantum-mechanical electronic ground state in the Born–Oppenheimer approximation. The electronic ground state is obtained within the density functional theory (DFT) [14,15]. The exchange-correlation functional used in our calculations includes gradient corrections (GC) to the local density approximation (LDA) [16,17] in the form proposed by Becke and Perdew [18,19]. Only the valence electrons are included explicitly in the calculation, while the atomic inner cores are frozen. The interaction between the valence electrons and the frozen core is described by soft first-principles pseudopotentials [20]. The single-particle Kohn–Sham wavefunctions are expanded on a plane-wave basis set with an energy cutoff of 20 Ry. The convergence relative to the energy cutoff has been discussed in previous papers [21,22]. The plane-waves expansion implies the use of periodic boundary conditions. We have used a simulation box of $19.1 \times 11.4 \times 11.4$ Å in order to reduce the interactions between images and to have an almost zero electron density at the cell boundaries. Finally, the time step for the molecular dynamics simulations is 0.15 fs.

In order to study the ground-state isomerization of the chromophore, we have included in the Hamiltonian an external torsional potential of the form:

$$V(\phi) = -\frac{V_0}{2} + \frac{V_0}{2}\cos(\phi) \qquad (1)$$

where ϕ is the C10–C11–C12–C13 dihedral angle. The forces derived from this field are just added to the ab-initio forces before each integration step. This field pushes the 11-*cis* compound toward the all-*trans* when V_0 has a positive value, and back from the all-*trans* to the 11-*cis* conformation when it is negative. The torsional motion of the chromophore backbone induced by this field occurs on a timescale which is much longer than the typical period of carbon–carbon bond oscillations. Therefore, the carbon–carbon bond lengths readjust 'quasi-adiabatically' to the instantaneous value of the dihedral angle. This allows us to explore the ground-state potential in the vicinity of the transition-state configuration.

3. Model

In the present work, we have modelled the chromophore with a retinylidene–ethylimine · HCl, following the model proposed in Ref. [21]. This model includes a number of structural constraints determined by Raman spectroscopy and solid-state magic-angle spinning NMR and the relevant interactions with the binding pocket. Scheme 1 shows the structure of the model; the atoms which have been kept fixed during the MD simulations are shown in bold type. The chromophore bears a positive charge in the tail region of the conjugated backbone. This excess positive charge is compensated by a negative counterion located in the vicinity of the chromophore. The primary counterion has been identified with the glutamate protein residue Glu^{113} [23]. In our model, the counterion is mimicked by a Cl^-, whose position has been fixed during the simulations. We have performed control simulations with a formiate group as a more realistic counterion, to test the relevance of details in the counterion structure. No substantial differences were observed in the two sets of simulations and we conclude that the Cl^- ion captures the essential electrostatic counterion–chromophore interaction. We have discussed the effects of the counterion on the structure of the chromophore in Ref. [21]. NMR data suggest that the C19 and C20 methyl groups experience steric interactions with the binding pocket [24]. Thus we have fixed the positions of the methyl groups in our molecular dynamics simulations. Similarly, we have blocked the C22 methyl group, which mimics the lysine side chain.

4. Results

Starting with the optimized structure of 11-*cis*-retinylidene–ethylimine · HCl (Z hereafter), we have

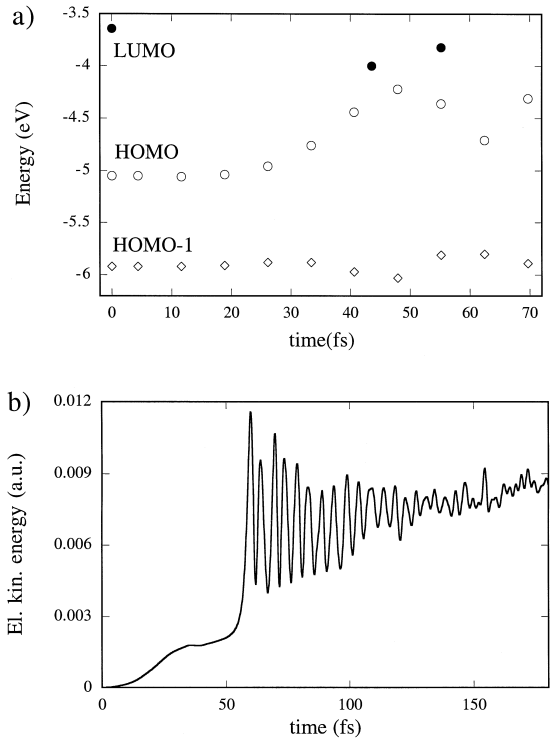

Fig. 2. (a) Evolution of Kohn–Sham eigenvalues for the two highest occupied (HOMO and HOMO-1) and the lowest unoccupied (LUMO) molecular orbitals in the presence of an external torsional field $V_0 = 100$ kcal/mol. The LUMO eigenvalues have been calculated only for a few selected atomic configurations. With increasing C10–C11–C12–C13 dihedral angle the HOMO–LUMO gap becomes smaller and a level crossing is observed after roughly 50 fs. The HOMO-1 eigenvalue is much less affected by the torsion of the chromophore. (b) Evolution of K, under the same conditions. When the level crossing occurs, the fictitious electronic kinetic energy presents a sharp increase due to the exchange of energy with the ionic degrees of freedom [12].

computed several CP-MD trajectories applying external torsional fields of various strengths for a simulation time of ≈ 130 fs (900 time steps). The torsional field drives the system through the transition state (TS) to the all-*trans* product (E thereafter), if the field is strong enough to overcome the isomerization energy barrier.

In Fig. 2a, we show the evolution of the two highest occupied Kohn–Sham eigenvalues and of the lowest unoccupied molecular orbital (LUMO) in the case of $V_0 = 100$ kcal/mol. As the dihedral angle C10–C11–C12–C13 increases, the HOMO–LUMO gap becomes smaller and a level crossing occurs when the transition state is reached. At the level crossing the fictitious kinetic energy associated with the electronic degrees of freedom shows a rapid increase (see Fig. 2b). This behaviour is due to a breakdown of the classical adiabaticity in the CP dynamics and to a dynamical instability in the oscillating motion of the electronic subsystem. The relation between the behaviour of the fictitious kinetic energy in a CP-MD simulation and the energy gap between occupied and unoccupied Kohn–Sham states is discussed in detail in Ref. [12].

CP-MD simulations have been performed for four different values of the torsional field $V_0 = 60$, 80, 100 and 120 kcal/mol. After the level crossing has been reached, the external field was set to zero, and the system evolved under the effect of the internal forces only. A field of 60 kcal/mol induces a torsion of the molecule, but is not large enough to cause the isomerization, i.e. to overcome the energy barrier and cross the energy saddle point, within the time of the simulation. Notice that part of the torsional field energy is transferred to other degrees of freedom due to the non-adiabaticity of this dynamical process. Fields $\geqslant 80$ kcal/mol lead to the formation of the product E. The time the system takes to reach the transition state TS is shorter the larger the external field.

After setting the external field to zero, the system has been equilibrated for 1200 steps (≈ 175 fs) and subsequently cooled by a simulated annealing procedure (600 steps at 100 K, 600 steps at 30 K, 600 steps at 10 K and 200 steps of steepest descent minimization) in order to reach the minimum energy structure of the E product.

The back-isomerization of the all-*trans* product E to the 11-*cis* reagent Z has been induced by applying a negative torsional field. The transition state for the back-isomerization is denoted by TSb (see Fig. 1). MD simulations were performed with $V_0 = -60$, -80 and -100 kcal/mol for 900 time steps. A field of -60 kcal/mol is sufficient to drive the system to the 11-*cis* reagent Z, consistent with a lower energy barrier for the *trans*-to-*cis* back-isomerization. Moreover, the energy barrier for the back-isomerization is less steep than that for the direct *trans*-to-*cis* isomerization. This makes the back isomerization process less dissipative, and the energy of the external field is spent more efficiently in

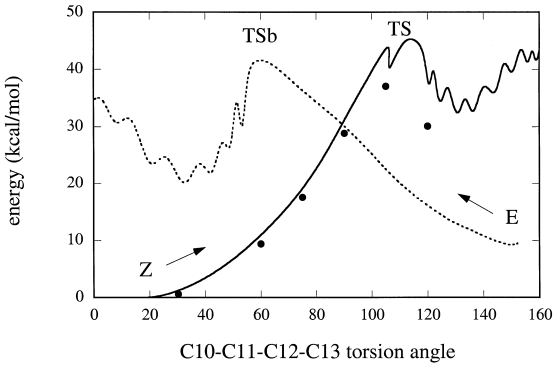

Fig. 3. Total energy E[p] along two MD trajectories as a function of the C10–C11–C12–C13 dihedral angle. The full and dotted lines correspond to MD simulations with external torsional fields of $V_0 = 80$ and $V_0 = -60$, respectively, prior to the simulated annealing that led to the final products. The full line refers to the *cis*-to-*trans* isomerization, whereas the dotted line corresponds to the *trans*-to-*cis* back-isomerization. The two isomerization processes were driven by different torsional fields because different barriers have to be overcome. The zero of the energy corresponds to the ground-state energy of the optimized 11-*cis* chromophore. The transition state is reached for different values of the dihedral angle C10–C11–C12–C13 for the direct and the inverse isomerization. For comparison, we have optimized the chromophore structure for fixed values of the dihedral angle (full dots). Even under these adiabatic conditions the *trans*-to-*cis* transition state is characterized by a dihedral angle larger than 90°.

climbing the energy barrier. The same simulated annealing procedure has been applied to find the minimum energy structure of the new Z reagent. The energies and the structures of the initial reagent Z and the new one obtained after the cycle are the same.

In Fig. 3 we show the total energy of the system as a function of the C10–C11–C12–C13 dihedral angle for the *cis*-to-*trans* and *trans*-to-*cis* isomerization. The level crossing is reached for two different values of the dihedral angle. However, these two states are characterized by similar bond patterns in the conjugated backbone. The total energy of the system was calculated along the MD trajectories and therefore the transition state might not have been approached adiabatically. In order to elucidate this point, we have selected a number of configurations along the isomerization path and optimized the chromophore structure constraining the C10–C11–C12–C13 dihedral angle. The corresponding values of the total energy are shown as full dots in Fig. 3. Even under adiabatic conditions the *cis*-to-*trans* transition state is reached for values of the C10–C11–C12–C13 dihedral angle larger than 90°, thus showing that the 'hysteresis' between the forward and backward transitions cannot be attributed to kinetic effects. Fig. 4 shows the bond lengths along the conjugated chain for the initial reagent Z, the product E and the two transition states for the direct and the inverse isomerization processes. The reagent Z presents a clear bond alternation, except for the terminal region of the conjugated chain in the vicinity of the NH group. This conjugation defect is induced by the excess positive charge borne by the chromophore (see discussion below). The product E also presents the conjugation defect in the terminal region of the backbone, but much more delocalized along the chain. This is consistent with previous calculations [21] and with NMR experiments [26].

The ionic temperatures of the TS and TSb configurations are rather high (220 and 150 K, respectively) and displacements of the ions due to finite temperature make the comparison of the two structures less straightforward. Nevertheless, remarkably similar features have been observed in the bond alternation patterns. In TS and TSb the conjugation defect is displaced toward the head of the molecule, and centered on C9. The displacement of the conjugation defect results in the inversion of the bond alternation in the tail of the molecule (Fig. 4a). The two transition states TS and TSb present different distributions of dihedral angles but the same bond alternation patterns. Thus, the transition state is not characterized by a specific C10–C11–C12–C13 dihedral angle, which is usually assumed as the relevant reaction coordinate, but by a specific distribution of bond lengths, which reflects the displacement of the conjugation defect. We notice that the C11–C12 bond at the transition state is considerably elongated. This appears to be a necessary condition for the isomerization to occur. This result is consistent with recent ab-initio studies of a smaller molecular fragment [27].

The bond alternation defect is induced by the excess positive charge borne by the chromophore [13]. In Fig. 4c we show the total electron charge on the carbon–carbon bonds for Z and TS. The electron charge localized on the bonds has been calculated using the electron localization function (ELF) [28,25]

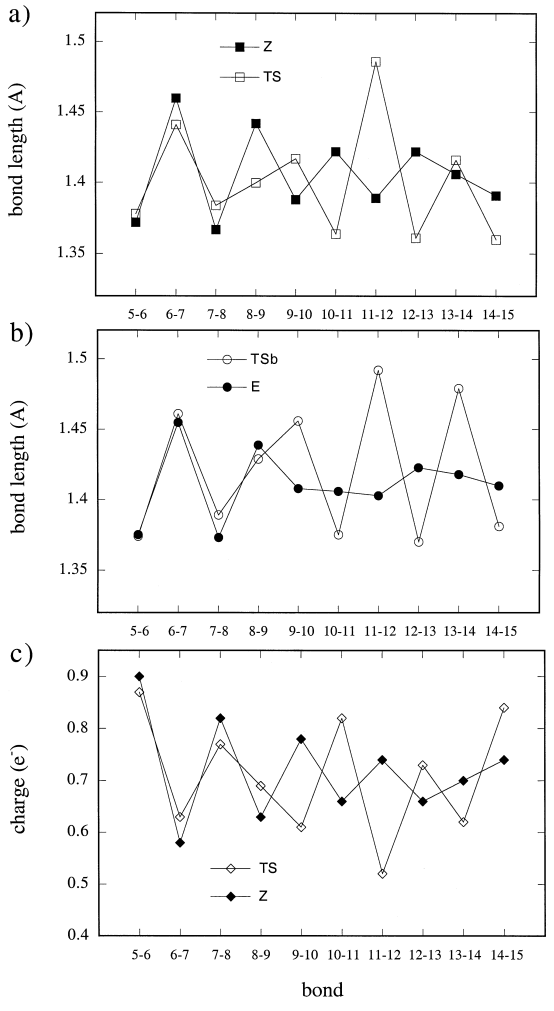

Fig. 4. Carbon–carbon bond lengths along the chromophore backbone. (a) The bond alternation of the 11-*cis* configuration (Z, full squares) shows a conjugation defect in the vicinity of the Schiff base. In the transition state (TS, open squares) the conjugation defect is located in the region of C9. The displacement of the conjugation defect induces an inversion of the bond alternation pattern in the tail of the molecule, whereas the bond alternation in the proximity of the ring is not affected. (b) The transition state for the back-isomerization (TSb, open circles) presents the same bond alternation of TS, with the conjugation defect located on C9. In the final all-*trans* configuration (E, full circles) the bond alternation is smaller than in the initial Z structure, consistent with a more delocalized conjugation defect. (c) Electron charge on the carbon–carbon bonds for the 11-*cis* structure (Z, full diamonds) and for the transition state (TS, open diamonds). The charge has been integrated in (bond) basins defined by the interval 0.9–1.0 of the electron localization function (ELF) [25]. The charge distribution reflects the bond alternation pattern. The displacement of the excess positive charge in the TS structure corresponds to the displacement of the conjugation defect pointed out in panel (a).

as a weighting function in the charge integration. This approach allows computing the charge within selected regions of maximum electron localization, particularly the bond attractors [25]. We have defined these regions as those with ELF between 0.9 and 1, bearing in mind that the ELF function ranges from 0, for regions of low localization, to 1 for regions with maximum localization. A comparison between Fig. 4a and Fig. 4c shows that the displacement of the defect in TS is associated with the displacement of the charge along the conjugated chain. The changes in the integrated charge on these bond basins correspond to the evolution of the bond alternation along the chain during the isomerization.

In our CP-MD simulations, the torsional field was set to zero after overcoming the energy barrier, i.e. in correspondence to the transition state. Thus, the subsequent evolution of the system toward the product E is a simulation of the chromophore relaxation after the non-radiative transition from the excited-state to the ground state potential. In Fig. 5 we report the differences between adjacent C–C bond lengths calculated from the ionic trajectories during the CP-MD simulation. As the system approaches the transi-

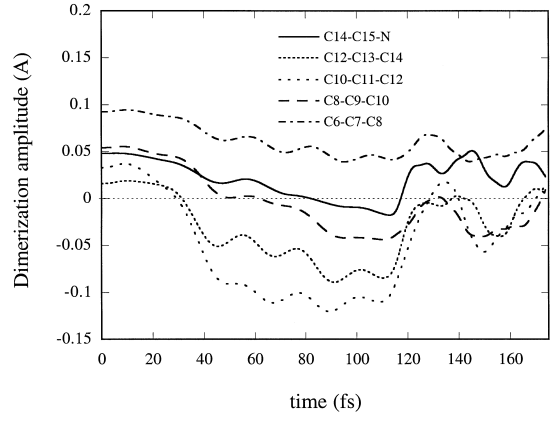

Fig. 5. Dimerization amplitudes (defined as the difference between adjacent C–C bond lengths) as a function of time for the direct 11-*cis* to all-*trans* isomerization induced by an external torsional field $V_0 = 80$ kcal/mol. The diffusion of the conjugation defect and the associated charge towards the ring results in an inversion of bond alternation pattern. The transition state, characterized by an inversion of the bond alternation pattern in the region C9–C15, is reached in about 110 fs. When the system relaxes to the E all-*trans* structure, the bond alternation pattern is recovered, but with smaller dimerization amplitudes.

tion state TS, the conjugation defect is displaced toward the ring, causing a bond alternation inversion in the fashion of a propagating charged soliton. The torsional field was set to zero after 110 fs. When the molecule relaxes toward the all-*trans* product E, the conjugation defect coherently returns to the tail of the molecule. The coherent propagation of this defect is associated with a propagation of the excess positive charge. The dynamics of a positively charged soliton along the backbone of a protonated Schiff base of retinal has been studied in Ref. [13], where it was shown that the propagation of the soliton was coupled to a slow collective vibrational mode of the chromophore. Damping of the soliton was attributed to coupling with out of plane vibrational degrees of freedom due to non-planarity of the chromophore. The present study shows that a soliton propagation is intimately connected with the chromophore relaxation toward the photoproduct. Femtosecond pump–probe experiments have revealed non-stationary coherent vibrational motion in the ground state of the photoproduct [7]. We suggest that these transient coherent vibrations may be related to the soliton oscillations along the conjugate backbone.

5. Conclusions

In this Letter we present a Car–Parrinello molecular dynamics study of the ground-state isomerization of rhodopsin. We have added to the ab-initio interatomic forces an external torsional potential on the C10–C11–C12–C13 dihedral angle. This external field drives the chromophore along the reaction coordinate over the isomerization energy barrier. We have characterized the transition states for the direct (*cis–trans*) and inverse (*trans–cis*) isomerization. These two states present different distributions of dihedral angles but the same characteristic bond length pattern. In the transition state the C11–C12 bond is considerably elongated and the conjugation defect is displaced from the Schiff base toward the head of the retinal. The displacement of the bond alternation defect corresponds to displacement of the excess positive charge borne by the chromophore. Relaxation of the system from the transition state to the all-*trans* photoproduct (bathorhodopsin) induces a propagation of the positively charged conjugation defect in the fashion of a charge soliton.

Acknowledgements

We acknowledge a supercomputer grant at the SARA national computing facility in Amsterdam.

References

[1] R.R. Birge, Biochim. Biophys. Acta 1016 (1990) 293.
[2] J. Lugtenburg, R.A. Mathies, R.G. Griffin, J. Herzfeld, Trends Biochem. Sci. 13 (1988) 388.
[3] R.W. Schoenlein, L.A. Peteanu, R.A. Mathies, C.V. Shank, Science 254 (1991) 412.
[4] F. Boucher, R. Leblanc, Photochem. Photobiol. 41 (1985) 459.
[5] G.A. Schick, T.M. Cooper, R.A. Holloway, L.P. Murray, R.R. Birge, Biochemistry 26 (1987) 2556.
[6] T.M. Cooper, Nature 282 (1979) 531.
[7] Q. Wang, R.W. Schoenlein, L.A. Peteanu, R.A. Mathies, C.V. Shank, Science 266 (1994) 422.
[8] R.B. Barlow, R.R. Birge, E. Kaplan, J.R. Tallent, Nature 366 (1993) 64.
[9] R.R. Birge, R.B. Barlow, Biophys. Chem. 55 (1995) 115.
[10] R. Car, M. Parrinello, Phys. Rev. Lett. 55 (1985) 2471.
[11] G. Galli, A. Pasquarello, in: M.P. Allen, D.J. Tildesley (Eds.), Computer Simulation in Chemical Physics, Kluwer, Amsterdam, 1993, p. 261.
[12] G. Pastore, E. Smargiassi, F. Buda, Phys. Rev. A 44 (1991) 6334.
[13] F. Buda, H.J.M. de Groot, A. Bifone, Phys. Rev. Lett. 77 (1996) 4474.
[14] R.G. Parr, W. Yang, Density Functional Theory of Atoms and Molecules, Oxford University Press, New York, NY, 1989.
[15] R.O. Jones, O. Gunnarson, Rev. Mod. Phys. 61 (1989) 689.
[16] J.P. Perdew, A. Zunger, Phys. Rev. B 23 (1981) 5048.
[17] D.M. Ceperley, B.J. Alder, Phys. Rev. Lett. 45 (1980) 566.
[18] A.D. Becke, Phys. Rev. A 38 (1988) 3098.
[19] J.P. Perdew, Phys. Rev. B 33 (1986) 8822.
[20] D. Vanderbilt, Phys. Rev. B 43 (1990) 7892.
[21] A. Bifone, H.J.M. de Groot, F. Buda, J. Phys. Chem. B 101 (1997) 2954.
[22] A. Bifone, H.J.M. de Groot, F. Buda, Chem. Phys. Lett. 248 (1996) 165.
[23] T.P. Sakmar, R.R. Franke, H.G. Khorana, Proc. Natl. Acad. Sci. USA 86 (1989) 8309.
[24] P. Verdegem, P. Bovee-Geurts, W. de Grip, J. Lugtenburg, H.J.M. de Groot, submitted.
[25] B. Silvi, A. Savin, Nature 371 (1994) 683.
[26] S.O. Smith, J. Courtin, H.J.M. de Groot, R. Gebhard, J. Lugtenburg, Biochemistry 30 (1991) 7409.
[27] M. Garavelli, P. Celani, F. Bernardi, M.A. Robb, M. Olivucci, J. Am. Chem. Soc. 119 (1997) 6891.
[28] A.D. Becke, K.E. Edgecombe, J. Chem. Phys. 92 (1990) 5397.